Volume 17, Number 4, 2024. pp. 461-468

Jordan Journal of Physics

ARTICLE

Effect of Strain Rate and Temperature on Mechanical Properties of Silicon Nanowire: MD Simulation Studies

S. Barik, C. Bhramarjal and **S. S. Sarangi**

Department of Physics, VSSUT, Burla, 768018, India.

Doi: **https://doi.org/10.47011/17.4.9**

Received on: 02/03/2023; *Accepted on: 18/05/2023*

Abstract: Silicon nanowires are of immense importance to the scientific community because of their unique properties and wide range of applications. In this work, MD simulations using MEAM potentials are employed to investigate the impact of temperature and strain rate on various mechanical properties of an ultra-thin silicon nanowire with a diameter of 3 nm. To characterize the effect of strain rate, the nanowire is subjected to strain rates varying from 0.0005 ps^{-1} to 0.05 ps^{-1} at 300 K, while the temperature effect is examined by varying it in the range of 10-700 K at a constant strain rate of 0.005 ps^{-1}. Young's modulus, yield strength, yield strain, and fracture strain of nanowire are calculated based on the variation of stress with strain. The study shows that both strain rate and temperature significantly influence the elastic and plastic characteristics of the nanowire. The strength of the silicon nanowire increases with higher strain rates and lower temperatures. To validate the chosen potential model, the Young's modulus of bulk silicon is estimated, showing good agreement with experimental values.

Keywords: MD simulations, Silicon, Nanowire, Strain rate, Young's modulus.

PACS: 68.35.Fx; 68.35.Ja.

1. Introduction

Nanoscale structures have drawn significant attention due to their unique mechanical, magnetic, electrical, optical, thermal, and other properties [1-8]. Nanoscale structures, such as nanowires (NWs), exhibit properties distinct from bulk materials due to their high surface-to-volume ratios. At these nano-dimensions, surface stresses and crystal orientations are the key factors in defining the properties. Silicon nanowire (Si NW) is one of the sought-after semiconductor NWs which has a broad spectrum of applications including in biosensors [9, 10], resonators [11], transistors [12], thermoelectric [13, 14], and electrode materials for various energy storage devices [15]. Therefore, it is essential to investigate their mechanical properties under various physical conditions.

To characterize the mechanical behavior of silicon nanowires, it is desirable to understand their tensile deformation properties under different loading conditions. Sohn and co-workers experimentally demonstrated the impact of size on various mechanical properties of Si NW [16]. Zhu *et al.* studied Si NWs' deformation and fracture mechanisms using scanning electron microscopy (SEM) [17]. They showed that the Young's modulus decreased and fracture strength increased with the decrease in the diameter of the nanowire. Tang *et al.* combined transmission electron microscopy and molecular dynamics (MD) simulations to reveal the impacts of diameter, stress state, and loading condition during tensile testing [18]. Over the past few decades, numerous experimental studies have characterized the mechanical properties of

Corresponding Author: S. S. Sarangi **Email**: sssarangi_phy@vssut.ac.in

Si NWs [18-20]. However, due to their small size, tensile testing of NWs requires sophisticated instrumentation, and it is challenging to precisely apply and measure external loads and strain at the nanoscale.

MD simulation is a computational tool for controlling external loads while examining the effects of a variety of external parameters, such as temperature, size, and strain rate. Hence, it can be used to examine the mechanical characteristics of NWs at the atomic scale [21-23]. Ivashchenko *et al.* investigated the influence of strain rate on the deformation mechanisms of Si NWs and concluded that failure strength rises linearly with a rise in the strain rate [24]. Jing *et al* highlighted the significant impact of strain rate, temperature, and size on the tensile mechanical properties of Si NWs [25]. Kang *et al* reported that the fracture mechanism of Si NWs depends on both temperature and size [26]. Moreover, theoretical simulations have also shown that Young's modulus for Si NWs increases with diameter and decreases with rising temperature [26, 27]

This study aims to provide a comprehensive understanding of the effects of strain rate and temperature on the stress-strain deformation and mechanical properties of ultra-thin Si NWs. In this context, MD simulations were conducted using modified embedded atom method (MEAM) potentials to examine the uniaxial tensile mechanical properties of a cylindrical, diamond cubic Si NW with a diameter of 3 nm across a temperature range of 10-700 K and strain rates varying from 0.0005 to 0.05 ps^{-1}. Various mechanical properties (yield strength, yield strain, fracture strain, and Young's modulus) were calculated by analyzing stress and potential energy variation with respect to strain. To address the scarcity of quantitative data and establish a theoretical basis for the applicability of Si NWs, this study further investigates the influence of temperature and strain rate on mechanical properties by analyzing atomic-level stress and strain variations.

2. Methodology

Large-scale Atomic/Molecular Massively Parallel Simulator (LAMMPS) software was used to carry out the MD simulations [28]. For the bulk Si crystal simulation, a diamond-structured bulk Si box containing 8000 atoms was created. The dimensions of the simulation box are 5.43 nm along the X, Y, and Z axes, representing the lattice directions [1 0 0], [0 1 0], and [0 0 1], respectively. Periodic boundary conditions (PBCs) were applied along the three directions to obtain the bulk structure.

For the NW studies, a cylindrical diamond cubic Si NW with a length of 10 nm (along the Z-axis) and a diameter of 3 nm containing 3567 atoms was created. Here, PBC is applied only along the Z-axis (the direction of applied strain), while shrink-wrapped boundary conditions are applied along the X and Y axes to ensure the one-dimensional NW structure.

The NW is divided into three distinct regions along its length: two grip regions, each 1 nm long at either end, where atoms are fixed to their lattice points, and a central deformable region, 8 nm in length, which contains mobile atoms. These regions are illustrated in Fig. 1, which shows a schematic representation of the initial structure of the Si NW.

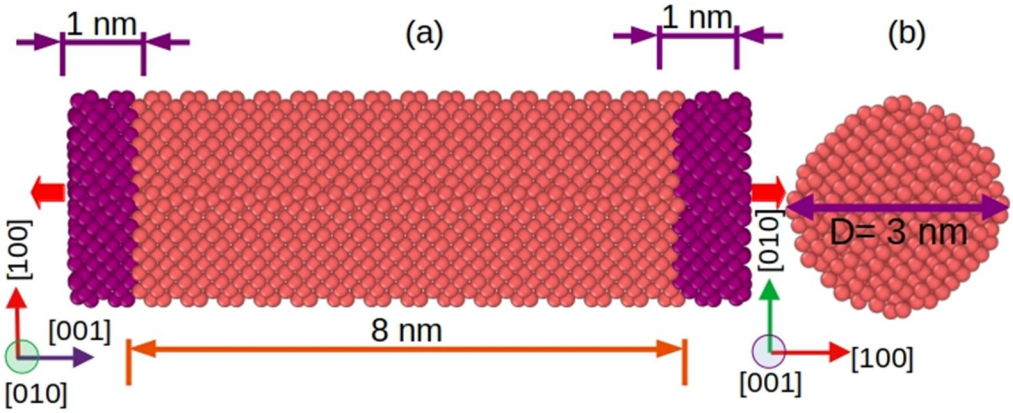

FIG. 1. (a) Side (lateral) view (b) top (transverse) view of a schematic diagram of the initial structure of the Si NW. Red horizontal arrows indicate the direction of application of tensile strain.

To begin the simulation at a given temperature, velocities are randomly assigned to the atoms according to a Gaussian distribution function. Then, the system is equilibrated for 1 ns in the NPT ensemble and the temperature is controlled by a Nosé-Hoover thermostat [29, 30]. After the equilibration period, a uniaxial tensile load at predetermined strain rates is applied along the Z-axis to create yielding and fracture in the NVT ensemble. The production time is about 1 ns. Velocity-Verlet algorithm is used for the calculations and the time step of integration is 1 fs. Visualization is carried out by using the Open Visualization Tool (OVITO) [31].

The NW is stretched along the Z-direction, and the corresponding component of the uniaxial tensile stress tensor is calculated by:

$$\sigma^{zz} = \frac{1}{\Omega}\left(-\sum_i m_i v_i^z v_i^z + \frac{1}{2}\sum_i \sum_{i \neq j} F_{ij}^z r_{ij}^z\right) \quad (1)$$

where Ω is the volume of the system, m_i is the mass, v_i is the velocity of the atom i, and F_{ij} and r_{ij} are the force and distance of separation between atoms i and j. The tensile strain along the Z-direction, e_{zz}, is determined by:

$$e_{zz} = \frac{L_z - L_0}{L_o} \quad (2)$$

where L_z is the instantaneous length under tension and L_0 is the initial length of the NW.

Interatomic potential plays a pivotal role in MD simulations and selection of it is crucial. Baskes extensively developed MEAM potential parameters to extend the embedded atom model (EAM) to account for bonding directionality [32-34]. Here, MEAM parameters developed by Lee et al. [32] are used for Si-Si interactions. In the MEAM model, the total energy is represented as:

$$E = \sum_i \left[F_i(\bar{\rho}_i) + \frac{1}{2}\sum_{j(\neq i)} S_{ij}\phi_{ij}(R_{ij})\right] \quad (3)$$

where F_i denotes the embedding function, ρ_i represents the background electron density at site i, S_{ij} is the screening function, and $\varphi_{ij}(R_{ij})$ stands for the pair interaction term between atoms i and j separated by a distance R_{ij}.

3. Results and Discussion

3.1. Simulation of the Bulk Si Crystal

The variation of stress with respect to strain is commonly used to calculate various mechanical properties of materials. Figure 2 depicts the stress-strain graph for bulk silicon at 300 K and 0.005 ps^{-1} strain rate.

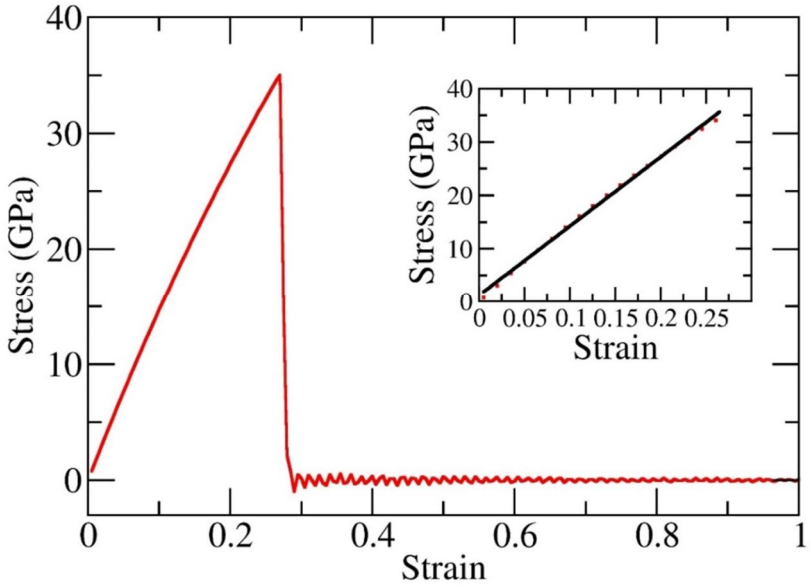

FIG. 2. Variation of stress with respect to strain for bulk silicon at 300 K temperature and strain rate of 0.005ps^{-1}. The inset shows a linear fit for the calculation of Young's modulus.

The figure illustrates that stress initially increases linearly with strain, indicating elastic deformation. In the elastic region, stress reaches a peak of 34.96 GPa (yield strength) at a strain of 0.270 (yield strain). Beyond this point, stress rapidly drops to zero as strain increases, indicating fracture. The slope of the stress-strain curve in the elastic region gives the Young's modulus, shown in the inset of Fig. 2. The calculated Young's modulus for bulk silicon at 300 K and a strain rate of 0.005 ps^{-1} is 129.6

GPa, closely matching the experimentally measured value of 130 GPa [35].

The effects of strain rate and temperature on the uniaxial tensile mechanical properties of Si NW are explained in the following sub-sections.

3.2 Effect of Strain Rate on Si NW

The nanowire is initially energy-minimized and then thermally relaxed at 300 K. After full relaxation, the Si NW is subjected to tensile loading along the axial direction (Z-axis) at different strain rates ranging from 0.0005 to 0.05 ps^{-1}. The corresponding stress vs. strain curves are shown in Fig. 3. It is observed from the graph that, for all strain rates, stress initially varies linearly with strain, indicating elastic deformation. The curves in this linear region are almost overlapping, which means Young's modulus is nearly independent of the strain rate. Beyond the elastic region, stress abruptly decreases, indicating fracture and confirming the brittle nature of the Si NW, as noted by other researchers [17, 20, 21].

The strain rate significantly influences the stress-strain curves beyond the elastic limit. Notably, as the strain rate increases, both fracture strain and yield strength increase. Table 1 provides the estimated values of Young's modulus, yield strength, yield strain, and fracture strain at each strain rate.

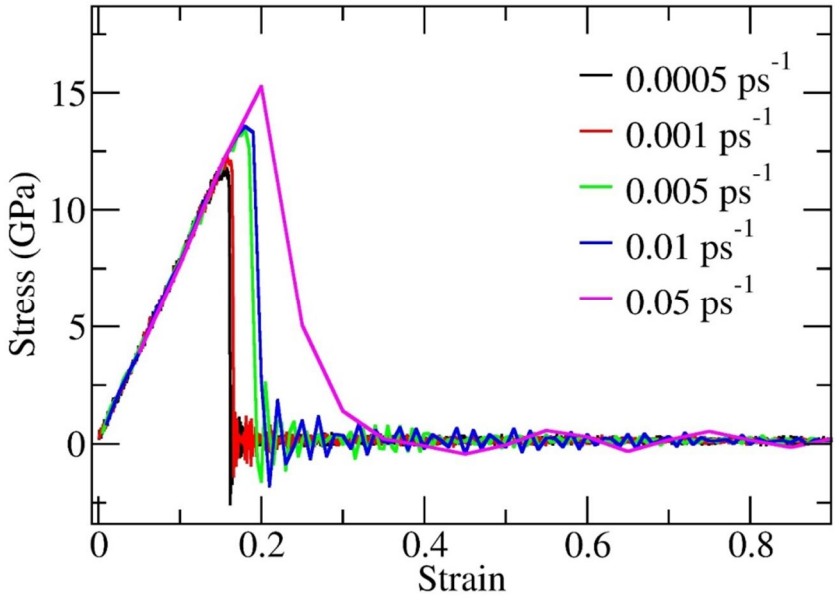

FIG. 3. Stress vs. strain curves of Si NWs at 300 K for different strain rates.

TABLE 1. The calculated values of mechanical properties at various strain rates for the Si NW at 300 K.

Strain rate (ps^{-1})	Young's modulus (GPa)	Yield strength (GPa)	Yield strain	Fracture strain
0.0005	77.73	11.7993	0.155	0.161
0.001	77.086	12.2578	0.156	0.165
0.005	75.85	12.480	0.175	0.187
0.01	77.453	13.452	0.18	0.205
0.05	76.773	15.2636	0.2	0.386

Figure 4 depicts the variation in potential energy of the Si NW as a function of strain for different strain rates at 300 K. Initially, potential energy rises linearly with strain, then drops steeply before gradually rising again. The first drop in the potential energy curve indicates the breaking of bonds and disruption of the crystal structure of the Si NW. It is also observed that the first drop in the potential energy curves shifts towards higher strain values with the increase in strain rate, which is consistent with the first peak positions of the corresponding stress-strain curves.

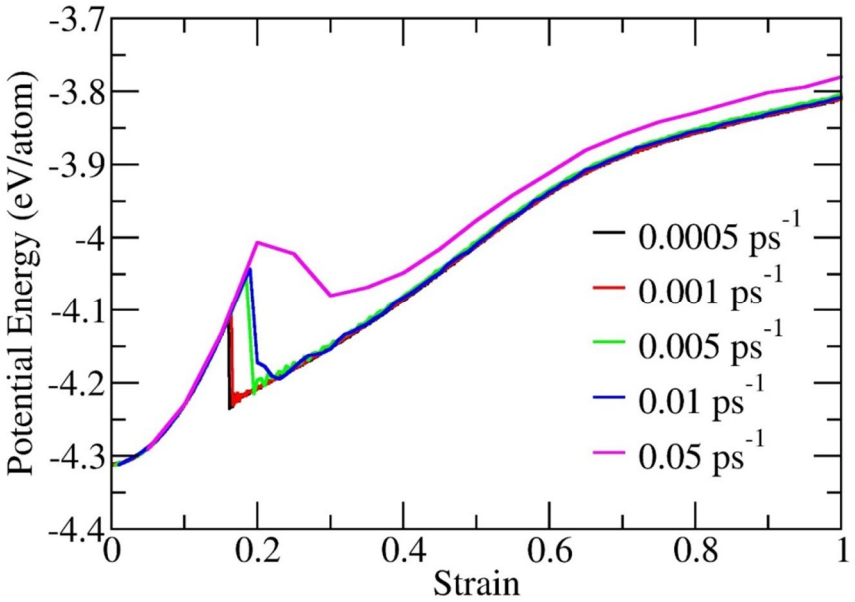

FIG. 4. Potential energy vs. strain curves at various strain rates of the Si NW at 300 K.

3.3 Effect of Temperature on Si NW

Kinetic energy determines the momentum and thermal excitations of the system, whereas potential energy assists in the investigation of the mechanical characteristics. Figure 5 depicts potential energy vs. strain curves for the Si NW at various temperatures ranging from 10 to 700 K. The elastic area of the potential energy curve increases monotonically with respect to strain, then dips rapidly, indicating the end of the elastic zone. Finally, when strain increases, the potential energy approaches a limiting value. Breaking of NW occurs when the potential energy value decreases below this limit. It is observed that with an increase in temperature, the potential energy of the system increases, and the strain at which the first peak appears also shifts to the left side of the graph (Fig. 5).

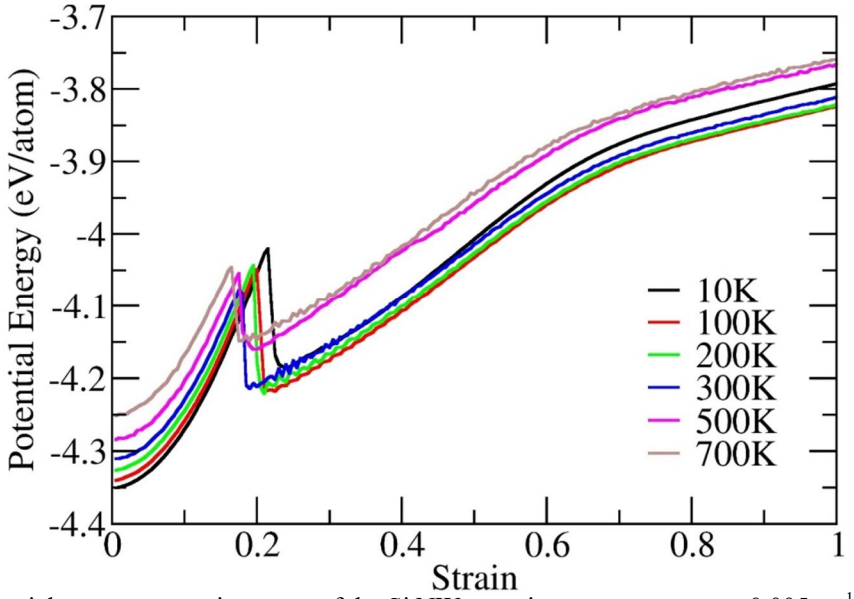

FIG. 5. Potential energy vs. strain curves of the Si NW at various temperatures at 0.005 ps^{-1} strain rate.

The temperature has a significant impact on the nanowire's tensile deformation behavior. To characterize the temperature effect on the mechanical properties of the Si NW, the stress versus strain curves in a temperature range of 10-700 K at 0.005 ps^{-1} strain rate are obtained and shown in Fig. 6. It is observed that the deformation of the NW gets accelerated with increase in temperature. Because greater temperatures cause atoms to oscillate more, massive dislocations are formed in weaker nanowires. As a result, the higher temperature causes the nanowire to fail prematurely. The attractive force between Si atoms decreases as temperature rises, causing atoms to drift from their equilibrium positions. Hence, the stress on the nanowire reduces at the same strain, resulting in lower Young's modulus and decreased yield strength, yield strain, and fracture strain. At higher temperatures and the same strain level, the number of displaced atoms and lattice defects rises, causing the NW to reach its ultimate stress point more quickly, thus decreasing yield strength. Thermal softening is evident as tensile stress decreases with temperature.

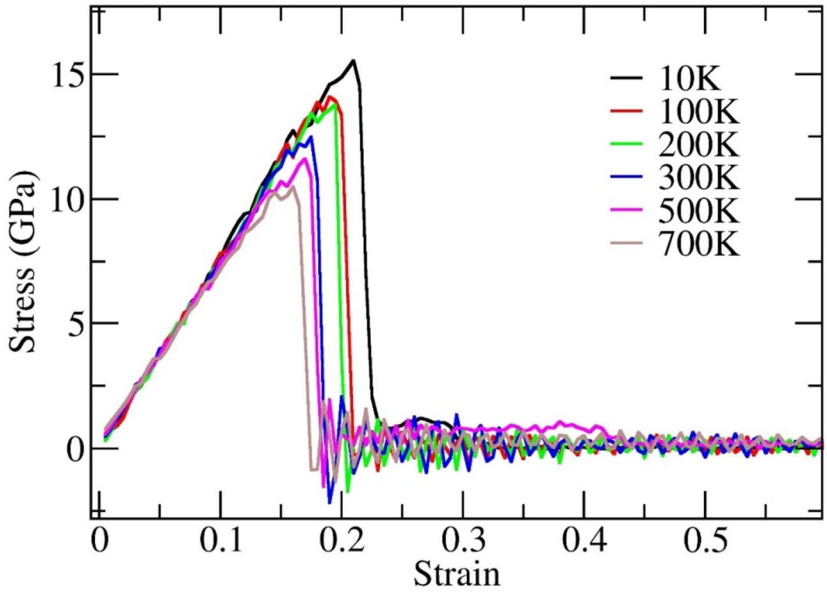

FIG. 6. Stress vs. strain curves of the Si NW for different temperatures at 0.005 ps^{-1} strain rate.

Figure 7 illustrates atomic configurations in the Si NW during tensile deformation at 300 K and 0.005 ps^{-1} strain rate. In Fig. 7(a), the Si NW, initially in a diamond cubic crystal structure, is shown after relaxation without loading. At a strain of 0.155, the NW reaches its elastic deformation limit (the first peak in the stress-strain graph), appearing elongated with a narrowed middle, as seen in Fig. 7(b). Plastic deformation begins beyond yield strain; at this stage, the NW surface fractures, planes slide along the cracking area, and atoms shift from their equilibrium positions. Figure 7(c) shows the NW at fracture strain (0.187), where it has broken into two separate parts. Table 2 lists the calculated mechanical properties of the Si NW at different temperatures.

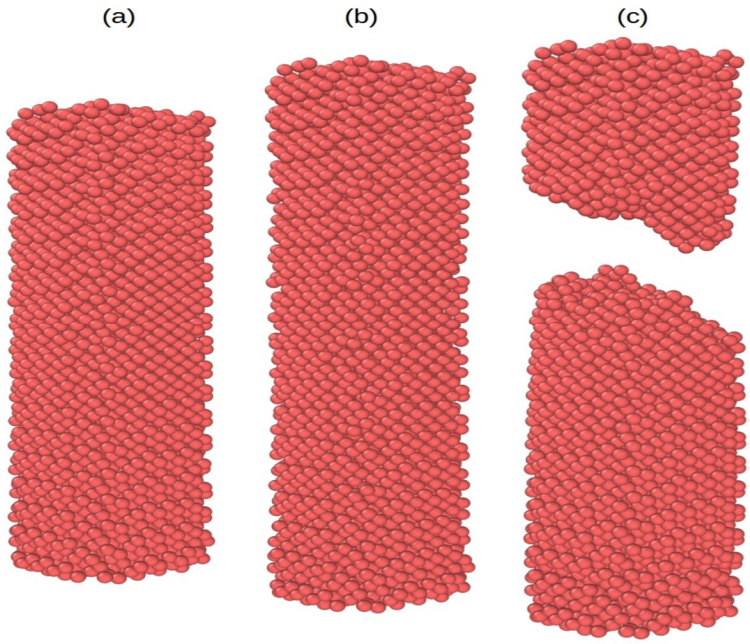

FIG. 7. Atomic configurations of the Si NW at 300K and 0.005 ps^{-1} strain rate (a) Original state, strain = 0. (b) Tensile state, Strain = 0.155. (c) Fracture state, strain = 0.187.

TABLE 2. The quantitative data on mechanical properties at various temperatures for the Si NW 0.005 ps^{-1} strain rate.

Temperature (K)	Young's modulus (GPa)	Yield strength (GPa)	Yield strain	Fracture strain
10	79.036	15.528	0.210	0.304
100	77.021	14.064	0.195	0.205
200	76.89	13.752	0.190	0.203
300	75.85	12.480	0.175	0.187
500	71.984	11.617	0.170	0.183
700	67.812	10.489	0.160	0.174

4. Conclusion

In this research work, the impact of strain rate and temperature on the mechanical properties of Si NWs was explored using MD simulations with the MEAM potential. The results reveal that strain rate and temperature distinctly influence various mechanical properties of the NWs. It is observed from our results that the yield strength, yield strain, and fracture strain increase with an increase in strain rate, whereas Young's modulus remains unaffected. Temperature has an equally important influence on the mechanical characteristics of the Si NW as it affects both the elastic and plastic characteristics profoundly. With an increase in temperature, Young's modulus, yield strength, yield strain, and fracture strain of the NW are found to decrease. These results show that with an increase in strain rate and decrease in temperature, the strength of the Si NW increases. Other factors, including size and orientation, also influence the mechanical properties of NWs, and we are currently exploring these in further research. The precise numerical values obtained in this study can aid experimentalists and guide future research in silicon nanomaterial applications.

Acknowledgment

The authors are thankful to the honorable vice chancellor of VSSUT, Burla, India, for providing the necessary facilities to carry out this research.

References

[1] Lieber, C. M., MRS Bull., 28 (7) (2003) 486.

[2] Cui, Y., Wei, Q., Park, H., and Lieber, C. M., Science, 293 (2001) 1289.

[3] Beckman, R. et al., Science, 310 (5747) (2005) 465.

[4] Canham, L. T., Appl. Phys. Lett., 57 (1990) 1046.

[5] Sarangi, S.S. et al., Indian J. Phys., 91 (2017) 853.

[6] Samantaray, M. P. and Sarangi, S. S., Mater. Proc., 46 (20) (2021) 10861.

[7] Samantaray, M. P. and Sarangi, S. S., Indian J. Phys., 96 (2022) 2285.

[8] Samantaray, M. P. and Sarangi, S. S., Int. Jour. Nanosci., 22 (1) (2023) 2250052-SA119.

[9] Ahmad, R., Mahmoudi, T., Ahn, M. S., and Hahn, Y.B., Biosens. Bioelectron, 100 (2018) 312.

[10] Buitrago, E., Badia, M. F. B., Georgiev, Y. M., Yu, R., Lotty, O., Holmes, J. D., Nightingale, A. M., Guerin, H. M., and Ionescu, A. M., Sens. Actuators B Chem., 199 (2014) 291.

[11] Čalnerytė, D., Rimavičius, V., and Barauskas, R., Acta Mech., 230 (2019) 1907.

[12] Ziegler, A. and Luisier, M., IEEE Trans. Electron. Devices, 65 (4) (2018) 1298.

[13] Lee, S., Kim, K., Kang, D. H., Meyyappan, M., and Baek, C. K., Nano Lett., 19 (2019) 747.

[14] Li, H.-P. and Zhang, R.-Q., Chin. Phys. B., 27 (3) (2018) 036801.

[15] Zhou, G., Xu, L., Hu, G., Mai, L., and Cui, Y., Chem. Rev., 119 (20) (2019) 11042.

[16] Sohn, Y. S., Park, J., Yoon, G., Song, J., Jee, S. W., Lee, J. H., Na, S., Kwon, T., and Eom, K., Nanoscale Res. Lett., 5 (2010) 211.

[17] Zhu, Y., Xu, F., Qin, Q., Fung, W. Y., and Lu, W., Nano Lett., 9 (11) (2009) 3934.

[18] Tang, D. M., Ren, C. L., Wang, M. S., Wei, X., Kawamoto, N., Liu, C., Bando, Y., Mitome, M., Fukata, N. and Golberg, D., Nano Lett., 12 (4) (2012) 1898.

[19] Han, X. D., Zheng, K., Zhang, Y. F., Zhang, X. N., Zhang, Z., and Wang, Z. L., Adv. Mater., 19 (2007) 2112.

[20] Gordon, M. J., Baron, T., Dhalluin, F., Gentile, P., and Ferret, P., Nano Lett., 9 (2) (2009) 525.

[21] Barik, S. and Sarangi, S. S., Mater. Proc., 56 (1) (2022) 60.

[22] Sarangi, S. S., Mater. Proc., 41 (2) (2021) 413.

[23] Barik, S. and Sarangi, S. S., Mol. Simul., 49 (4) (2023) 377.

[24] Ivashchenko, V. I., Turchi, P. E. A., and Shevchenko, V.I. Phys. Rev. B, 75 (8) (2007) 085209.

[25] Jing, Y. H., Meng, Q. Y., and Zhao, W., Physica E., 41 (4) (2009) 685.

[26] Kang, K. and Cai, W., Int. J. Plast., 26 (9) (2010) 1387.

[27] Zhao, D., Li, J., and Zhang, L., Crystals, 11 (9) (2021) 1010.

[28] Plimpton, S., J. Comp. Phys., 117 (1) (1995) 1.

[29] Nose, S., J. Phys. Condens. Matter, 2 (1990) SA115.

[30] Hoover, W. G., Phys. Rev. A, 31 (3) (1985) 1695.

[31] Stukowski, A., Model. Simul. Mater. Sci. Eng., 18 (1) (2009) 015012.

[32] Lee, B.-J., Calphad, 31 (1) (2007) 95.

[33] Baskes, M. I., Mater. Chem. Phys., 50 (2) (1997) 152.

[34] Lee, B. J., Shim, J. H. and Baskes, M. I., Phys. Rev. B, 68 (14) (2003) 144112.

[35] Hopcroft, M. A., Nix, W. D., and Kenny, T. W., J. Microelectromech. Syst., 19 (2) (2010) 229.